A Numerical Investigation of the Application of Compressed Sensing in Spherical Mode Filtering for Near- or Far-Field Antenna Measurements

Zhong Chen[1], Fellow AMTA, Stuart F. Gregson[2,3], Fellow AMTA, Yibo Wang[1], Member, AMTA, Rostyslav F. Dubrovka[3]
(1) ETS-Lindgren, Cedar Park, Texas, USA
(2) Next Phase Measurements, Garden Grove, California, USA
(3) Queen Mary University of London, London, U.K.

***Abstract*— This paper presents the results of an extensive numerical investigation into the spherical mode filtering method and the application of Compressed Sensing (CS) for near- or far-field two-dimensional antenna pattern measurements. This study is an extension of the authors' prior work [1, 2] that expands the findings to the generalized case. When measuring an antenna pattern at a near-, intermediate, or true far-field distance, spherical mode filtering of an intentional offset antenna very effectively removes parasitically coupled multipath reflections from the test environment. The CS algorithm further enhances this technique by allowing the data to be sampled on an irregularly spaced spherical grid comprising only a few percent of the measurement points required by a conventional equiangular, Nyquist sampled, spherical acquisition. This investigation uses full-wave three-dimensional computational electromagnetic simulated data to examine the spherical mode filtering technique, addressing questions about the mechanism of modal separation, *i.e.* the mode orthogonalization, and sparsification facilitated by the translation of origins of the measured antenna pattern to the measurement rotation center. Additionally, the paper discusses potential limitations of the approach, identifying scenarios where modal filtering may be less effective—issues previously noted for one-dimensional cylindrical mode filtering but not yet documented in existing open literature for the analogous 2-D spherical case.**

Index Terms*— *Compressed Sensing, Reflection Suppression, Sparse Sampling, Spherical Mode Filtering.

I. Introduction

Antenna pattern measurements are often affected by chamber reflections, which introduce multipath interference. A well-established technique to mitigate these effects is spherical mode filtering, typically implemented using an intentionally offset antenna [3-5]. This method hinges on the mathematical translation of the measured phase pattern back to the rotation center (for the far-field pattern data), which is a post-processing operation that reduces the Minimal Radial Extent (MRE), defined as the smallest radius enclosing the antenna's rotational path that is centered about the origin of the measurement coordinate system. Since the antenna's supported modes are constrained by this reduced MRE, genuine antenna modes are concentrated in the lower orders, while higher-order modes, those unsupported by the MRE, are attributed to multipath reflections. This gives rise to a critical question: under what conditions might scattering modes remain within the reduced MRE, thereby resulting in residual contamination that cannot be fully suppressed by mode filtering? Experimental approaches alone provide limited insight into this issue, as ideal reference data is rarely available, and isolating contributing parameters in a physical setup is inherently difficult. In contrast, numerical simulations offer a more controlled and systematic means of investigation [6] although they are computationally intensive. In the previous work [1], we demonstrated through numerical modeling that, in the one-dimensional (1D) cylindrical mode case, achieving clean separation and orthogonalization of antenna and scattering modes is challenging under certain circumstances, with residual effects persisting.

In this work, we extend the investigation to the two-dimensional (2D) spherical case to examine analogous physical phenomena. In [1], we showed that when the antenna rotates with an offset, tracing an arc, certain geometric alignments can influence the effectiveness of mode separation. Specifically, when the direction of antenna movement is tangential to the line bisecting the incident and scattered (interfering) waves, the resulting response from the interfering fields exhibit a more slowly varying interference pattern and, consequently, lower spectral frequency content. Under such conditions, the interfering modes may not be efficiently shifted to higher-order modes during the translation and mode filtering process. As a result, some residual scattering modes remain within the same spectral region as the antenna's own modes, even after the translation operation to the rotation center.

In the 2D case, we analyze several scenarios analogous to those explored in the 1D study, in which a plane wave impinges on a receiving antenna undergoing spherical rotation. Unlike the 1D case, multiple scanning topologies can be used to achieve full spherical coverage, each creating distinct interactions with the scattered field. As a result, the performance of spherical mode filtering can vary depending on the scan strategies employed. In this work, we investigated two scanning methods: (1) the conventional scan, where the elevation angle θ spans from 0° to 180°, and the azimuth angle ϕ from 0° to 360°; and (2) the alternate scan, where θ spans from 0° to -180°, with ϕ again covering 0° to 360° [9].

We consider two antenna types: one with equal front and back lobes (0 dB front-to-back ratio), and another with a pronounced front-to-back ratio of approximately 30dB. Following the methodology of the 1D study, we perform simulations with a lossy dielectric ground plane to represent a large reflective surface. Although such large reflectors represent extreme and

idealized scenarios rarely encountered in practical measurements, they provide a controlled and challenging environment for study. These test cases help yield clear, interpretable results that shed light on the broader strengths and limitations of spherical mode filtering. To the authors' knowledge, such an investigation into the effects of scan geometry and antenna directivity on 2D spherical mode filtering has not been documented in the existing open literature.

We then examine the application of Compressed Sensing (CS) to these datasets. In the far-field case, translating measurement coordinates back to the rotation center reduces the Maximum Radial Extent (MRE), which can potentially further sparsify the modal distribution [7]. However, this translation is generally not applicable in the near-field due to the breakdown of far-field assumptions. Since our practical objective is to apply CS to near-field scans, we perform CS prior to coordinate translation [2]. In this case, sparsity arises from the inherent modal structure of the antenna and scatterer, as well as from avoiding the oversampling that results from using uniform angular steps in θ and ϕ, which causes dense point spacing near the poles, rather than from additional data processing. We consider two offset distances: 0.3 m and 0.7 m. In both cases, we are able to accurately reconstruct the modal content, particularly the dominant coefficients associated with the antenna. After coordinate translation and filtering, the antenna patterns are successfully recovered using only ~5 percent of the original sampling points. These results demonstrate that Compressed Sensing is a viable and effective method for significantly reducing data acquisition time in spherical near-field measurements while preserving the fidelity of the reconstructed radiation pattern, with this also being true when in the presence of large, complex, scatterers.

II. Numerical Simulation Setup

NEC-2 [8] is used as the simulation engine. Two array antennas are modeled: the first is a single-layer dipole array with equal front and back lobes, and the second is an end-fire dipole array with an approximate 30 dB front-to-back ratio. Both operate at 10.2 GHz, consistent with previous studies. Fig. 1 illustrates the simulation setup. The NEC-2 ground plane feature (GN card) is used to model an infinite half-space scattering medium with a relative permittivity $\varepsilon_r = 3$ and conductivity $\sigma = 2$ S/m. The antenna is rotated about its local coordinate system (as shown in the figure), with an offset radius r, and is located at a height h above the half-space interface. The incident plane wave and the normal to the reflecting surface form an angle α.

As previously discussed, two rotational scanning schemes are considered. In the conventional scheme, θ spans from 0° to 180°, covering the "lower" half of the sphere. In the alternate scheme, θ spans from 0° to -180°, covering the "upper" half. In both cases, ϕ spans 0° to 360°. Although both schemes cover the entire angular space, their orientation relative to the reflecting surface differs. Crucially, this results in different interactions with the reflected field, as the following results will demonstrate.

III. Simulation Results

In the 1D case, it was shown that when the antenna moves along a direction that bisects the incident and reflected waves, the resulting interference pattern varies more slowly due to smaller phase difference variation along that path. Based on the test setup geometry, the angle at which this occurs can be predicted. For example, in the plane cut shown in Fig. 1, when the antenna's motion in θ follows lines that are parallel to the reflecting surface (as that bisects the two waves), as indicated by the two red lines, the reflection effects become the most challenging to filter out.

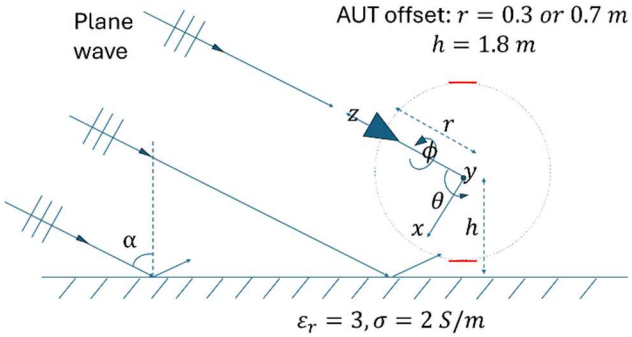

Fig. 1. Simulation setup. An infinite scatterer causes an interfering wave at angle α from the normal direction of the reflecting surface.

A. Case 1: Antenna with 0 dB front-to-back ratio

For the conventional sphere scan, which corresponds to the "lower" half, the antenna rotates in θ toward the reflecting surface. In this case, the lower red line in Fig. 1 is relevant. In this setup, we chose $\alpha = 25°$ and $h = 1.8$ m, and $r = 0.3$ m. At θ angle of approximately 155° (that is, 180°–25° from the z-axis where the antenna rotates to coincide with the bottom red line), we expect the mode filtering algorithm to have the greatest difficulty in removing reflected components. For the alternate sphere scan, representing the "upper" half, the top red line becomes the area of interest. Here, the critical angle is 25° from boresight.

Fig. 2 shows the reference pattern (obtained in in free space) and the difference between the mode filtered result and the reference. As seen, the angular regions with the largest deviation from the reference align well with the prediction. Fig. 3 presents the 1D pattern along the 0° elevation cut to more clearly illustrate the differences between the two scan strategies. One notable observation is that the maximum error differs between them: the dashed blue line shows a peak deviation of -18 dB for the conventional scan, compared to -15 dB for the alternate scan. This difference is expected, as the phase relationships between the incident and reflected waves are not necessarily symmetric in the two configurations. More broadly, some error remains in both cases due to mode mixing that persists even after coordinate translation and filtering. The averaged result shown in Figs. 2(d) and 3(c) is obtained by first averaging the patterns from both scan configurations, followed by translation to the rotation center and filtering. While this approach is intended to reduce overall error, in practice it tends to distribute local errors across the pattern. Ideally, one could selectively retain the better-performing regions from each scan to form a composite pattern. However, in practice, without prior knowledge of where the problematic regions are, such a strategy is difficult to implement. This remains an open area for future investigation.

Another key observation comes from examining the green trace in Fig. 3, which represents the raw data. The largest errors

occur at angles where the perturbed patterns vary slowly, corresponding to lower order modes. While the high-frequency ripples are effectively suppressed by the filtering process, these slowly varying components are more difficult to eliminate through coordinate translation and filtering, making them more persistent in the final processed pattern.

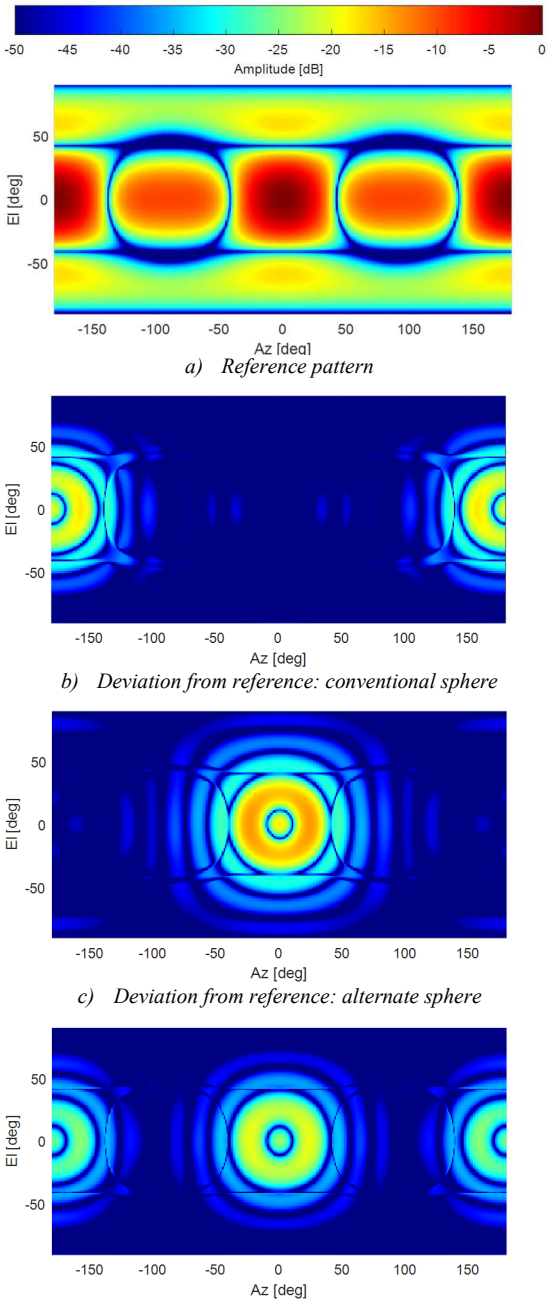

a) Reference pattern

b) Deviation from reference: conventional sphere

c) Deviation from reference: alternate sphere

d) Deviation from reference: average

Fig. 2. Filtered pattern differences from reference. Filtered results are obtained using incident plane wave in the presence of scatterer.

The spherical modal distribution data further supports the observation that residual energy remains in the lower-order modes even after coordinate translation. Fig. 4 presents the two-dimensional modal distributions for the TE (Q1) and TM (Q2) modes for the conventional sphere. After translation (shown in the right-hand plots), the energy shifts toward the lowest orders, as expected, but not all undesired components have moved away. Fig. 5 shows a cut along $m = 1$ for the translated modes, compared to the reference modal distribution. The dashed blue line indicates the difference between the translated, perturbed modes and the reference. Notably, while some higher-order content is suppressed, there is still significant energy belonging to perturbations remaining within the lower-orders (around 20 dB below the reference antenna levels). These residual components contribute to the distortions observed in the filtered radiation patterns shown in Figs. 2 and 3. The same observations can be made for the alternate sphere, as shown in Fig. 6 where there is also approximately 20 dB separation between the antenna modes the scattering modes.

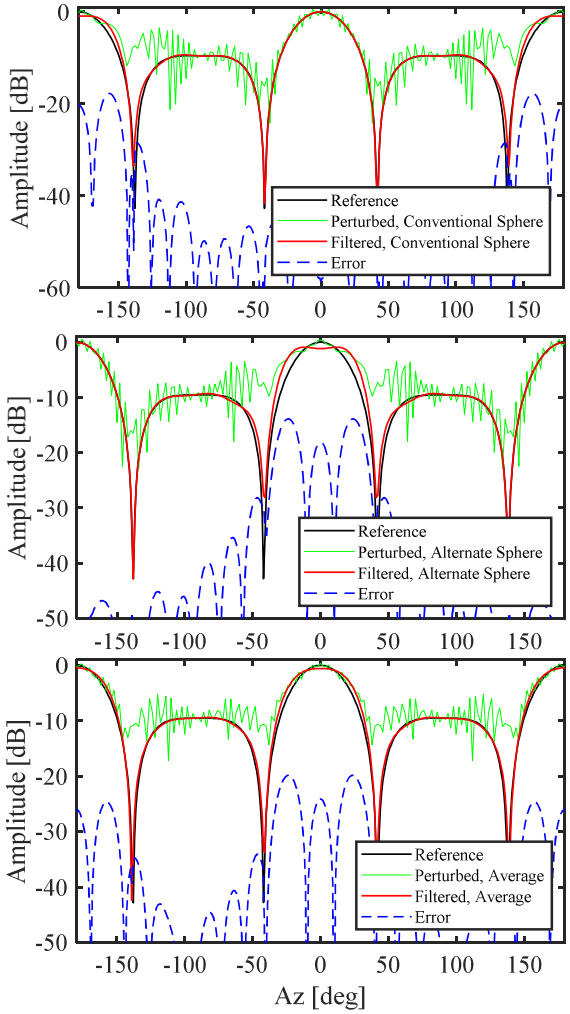

Fig. 3. Antenna pattern cut along 0° elevation, showing the perturbed, filtered, reference patterns and the difference between the filtered and reference pattern.

To further validate that the predicted angular regions follow the change of the reflected wave angle α, we adjust α to 67.5°. Fig. 7 shows the results for the two scan spheres. The results follow the prediction: the conventional scan shows the residual errors are largest near 112.5° (or 180°–67.5°) for the conventional sphere, and near 67.5° for the alternate scan. Again, the error levels are not the same for the two scan

geometries. Thus, this warrants further investigation in a future study on how best to select the scan strategy for a given setup or based on observations in the raw data, particularly when the direction of the strongest scattered wave is known or can be estimated.

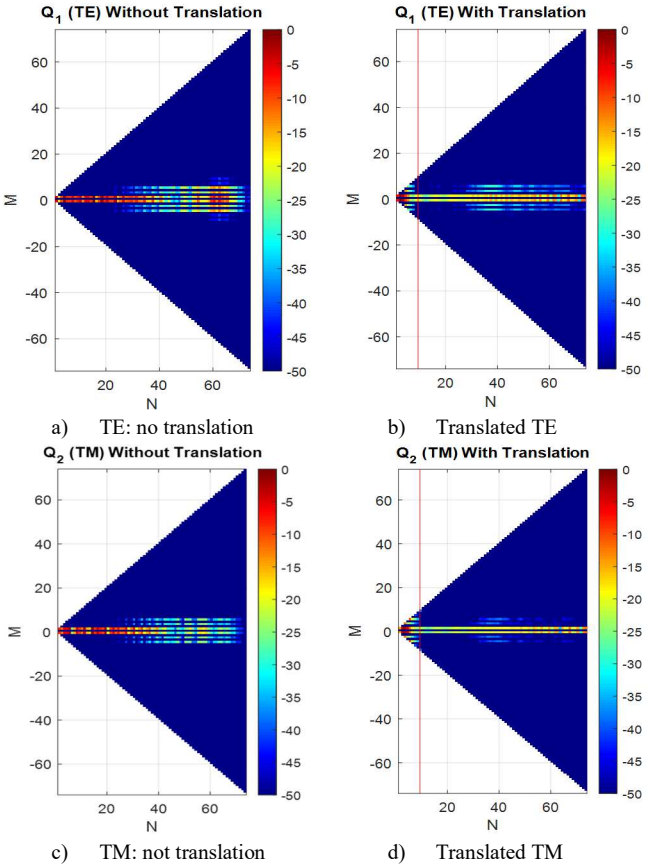

a) TE: no translation b) Translated TE

c) TM: not translation d) Translated TM

Fig. 4. Spherical modes for the conventional sphere for antenna with 0 dB front-to-back ratio and α=25°. The red vertical line indicates the filter cutoff.

B. Case 2: Endfire array antenna with ~30 dB front-to-back ratio

In the 1D case, we showed that the antenna pattern acts as a spatial filter that influences the level of perturbation, even though the angular regions where filtering is most difficult are primarily governed by the reflection geometry. In one example, at an angle where filtering was challenging, the reflected wave entered through a strongly attenuated back lobe. Under this condition, no persistent angular artifacts were observed. However, a high front-to-back ratio does not necessarily guarantee this favorable outcome. Here, we consider an antenna with a 30 dB front-to-back ratio and a reflected wave forming an angle α = 67.5°. Fig. 8 shows that the problematic regions appear, as expected, near 112.5° for the conventional scan sphere and around 67.5° for the alternate sphere. Both cases exhibit relatively high residual error levels of about -20 dB after filtering. A closer examination of the test geometry reveals that the reflected wave arrives from 180° minus twice α, which is 45° from the incident wave. At this angle, the antenna still exhibits a strong lobe in both scan configurations. In each case, the incident wave (at the problematic angles) and the reflected wave fall within the second lobe of the antenna pattern and are received at comparable power levels. As a result, the large front-to-back ratio does not help reduce the level of interference.

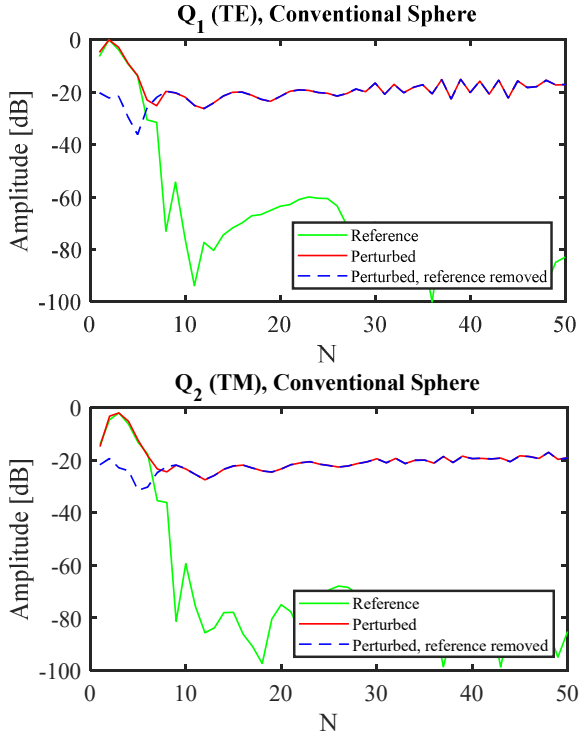

Fig. 5. Spherical modes corresponding to m = 1 cut of Fig. 4 for conventional sphere.

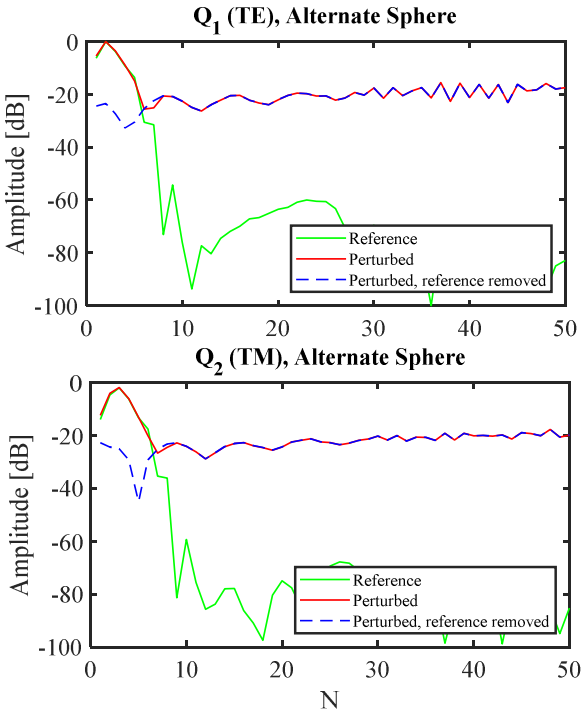

Fig. 6. Spherical modes corresponding to m = 1 cut of Fig. 4 for the alternate sphere.

An additional question concerns the impact of the offset distance on reconstruction quality. In the next experiment, we

increase the offset of the endfire antenna from 0.3 m to 0.7 m while keeping all other setup parameters unchanged. The goal is to evaluate whether this increase improves mode orthogonality or helps reduce residual scattering modes within the region occupied by the antenna modes. Fig. 9 presents the results. Only a marginal improvement is observed when increasing the offset from 0.3 m to 0.7 m. The larger offset leads to a greater Maximum Radial Extent (MRE), which in turn increases the Nyquist frequency and thus the required sampling density. However, this added complexity yields little practical benefit. For this type of error, increasing the offset does not appear to offer sufficient improvement to justify the higher sampling cost.

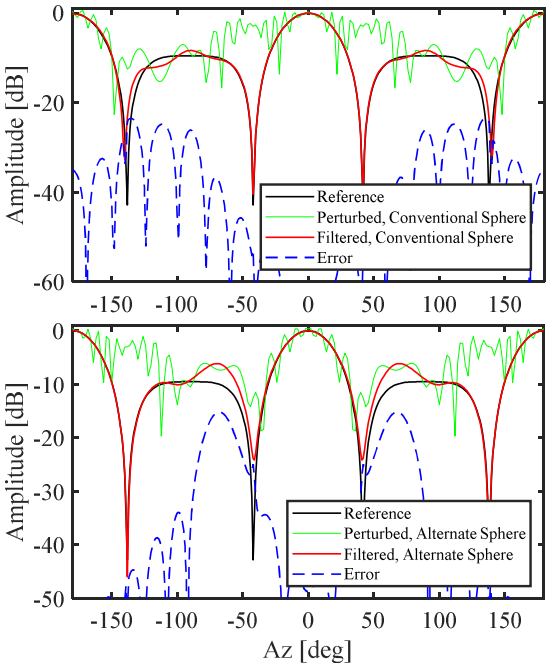

Fig. 7. Antenna pattern cut for α = 67.5° for (a) conventional and (b) alternate spheres.

IV. COMPRESSED SENSING

Traditional spherical scanning using Fast Fourier Transforms (FFT) requires equiangular sample spacing. This leads to excessive point density near the poles and results in approximately 100% oversampling [9]. In addition, most antenna radiation patterns exhibit symmetry and structural characteristics that promote sparsity within the spherical mode domain. As shown in Fig. 4, the significant coefficients within the triangular region defined by the Maximum Radial Extent (MRE) are primarily concentrated at lower *m* indices, with some additional sparsity observed along *n*. This intrinsic sparsity can be effectively exploited using CS. Rather than acquiring at or above the Nyquist rate using uniform steps, CS allows for the random selection of a much-reduced number of samples from our 1° dense dataset (random sampling is used to satisfy the Restricted Isometry Property requirement). For example, Fig. 10 shows a sampling pattern using only 5.2% of the data for the r = 0.7 m endfire array case discussed earlier.

In the 1D case, coordinate translation can further sparsify the modal distribution, especially when lower order antenna modes are well separated from higher order scattering modes. This helps concentrate energy into fewer dominant modes. Since 1D measurements are more commonly performed in the far- or quasi-far-field, where the assumptions required for translation are valid, coordinate translation was used in our earlier work [1, 4]. In contrast, 2D measurements are more commonly performed in the near-field, where the same assumptions do not hold. Although this study uses far-field simulation data, our practical focus is on enabling CS for near-field measurements. Therefore, we apply CS directly to the original data *without* coordinate translation.

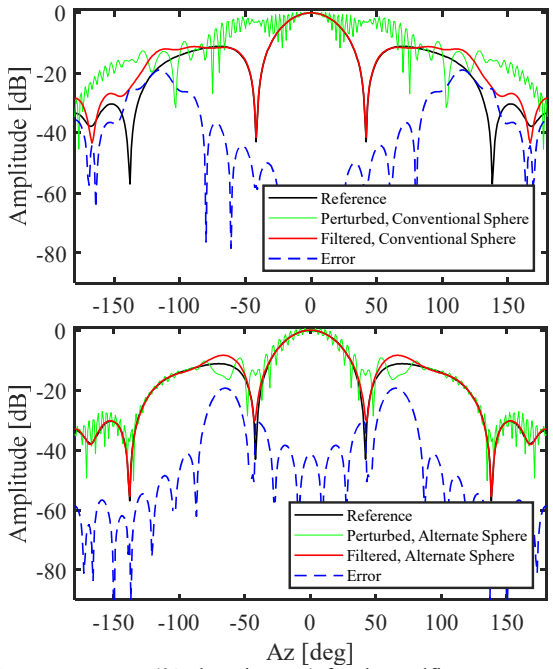

Fig. 8. Antenna pattern (0° elevation cut) for the endfire array antenna for α = 67.5° for (a) conventional and (b) alternate spheres.

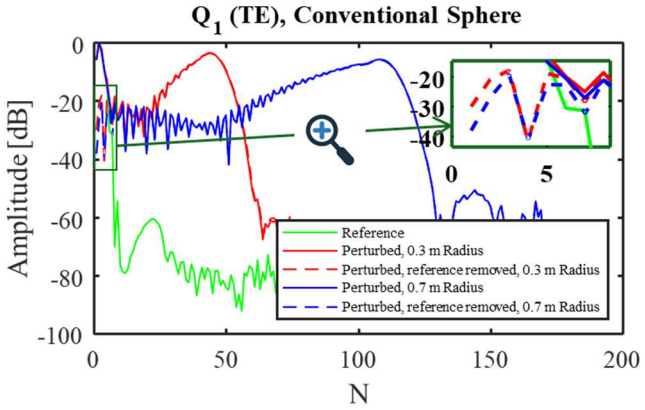

Fig. 9. TE mode (m=1 cut) for the endfire array antenna. α = 67.5°, conventional sphere, comparing offsets of 0.3 m and 0.7 m.

Fig. 11 shows the spherical modes with *m* = 1 for both the TE and TM coefficients. The dominant modes are clearly recovered using the CS approach, even with only 5.2 percent of the full dataset. While some reduction in sampling density is possible using a uniform grid and conventional FFT based processing, the figure shows that there is not much room for improvement. Resolving higher order modes, particularly when

the antenna is offset with a large radius, still requires dense angular sampling.

Fig. 12 presents the recovered patterns for both the 0.3 m and 0.7 m offset cases. Notably, for the 0.7 m case, the same number of sample points results in more severe under sampling, as the energy spreads into higher-order modes due to the larger offset. Despite this, the CS algorithm performs remarkably well in recovering the antenna pattern, particularly within the main lobe region. This also accounts for the slightly degraded performance for the 0.7 m case compared to the 0.3 m case.

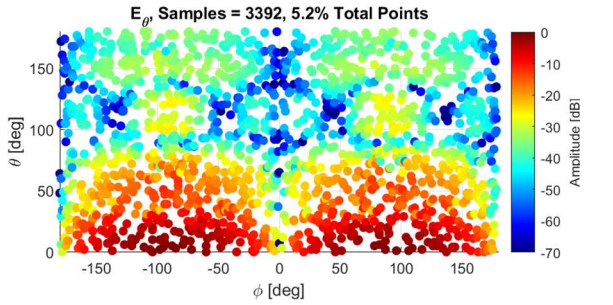

Fig. 10. Sampling points for the endfire array antenna used by CS. Magnitudes are displayed as a heat map.

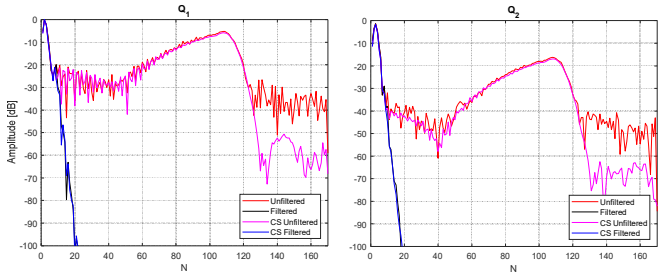

Fig. 11. Spherical modes (m=1) comparing regular processing (pink) and CS (red), corresponding to Fig. 10 (left: TE modes; right: TM modes).

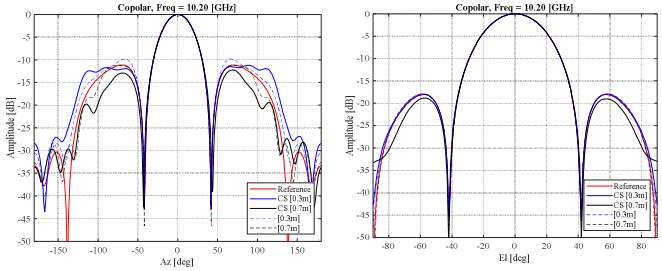

Fig. 12. Antenna pattern for the endfire array comparing CS and regular processing (left: azimuth cut; right: elevation cut).

V. Summary and Conclusion

This study extends previous 1D cylindrical work to 2D spherical measurements. We examined the effectiveness of spherical mode filtering using offset scans. Reflection-induced artifacts are most difficult to remove when the antenna movement direction results in minimal change in path length difference between the incident and reflected waves. This typically occurs when the antenna rotates through angles near the bisecting angle between the two wave paths, where the interfering signals become more coherent.

Different scan strategies produce different relationships between the interfering waves. This leads to variations in both the angular location and the levels of residual errors. While it is sometimes possible to predict the problematic regions based on the test geometry, this requires prior knowledge of the dominant scattering direction, which is often not available. The antenna pattern itself can help suppress reflected signals if the reflections arrive from low-gain directions. However, a high front-to-back ratio alone does not ensure that condition. Averaging results from two scan configurations can reduce local errors but may also distribute them more broadly. A better approach would be to selectively combine the more accurate parts from each scan. Identifying these regions without prior knowledge remains an open problem and is a subject for future research.

Compressed Sensing was also evaluated in this study. It successfully recovered the dominant spherical modes using a small percentage of measurement samples. This is possible because antenna patterns tend to be sparse in the spherical mode domain. Coordinate translation can improve sparsity in 1D measurements, but it does not generally apply to spherical near-field setups. Even without translation, Compressed Sensing performed well, especially in recovering the main beam region.

While the test cases in this study were specifically designed to stress the algorithm, they offer valuable insight into the conditions under which spherical mode filtering is most effective. The results offer practical guidance for future measurements.

References

[1] Z. Chen, Y. Wang, "A Numerical Investigation of the Application of Compressed Sensing in Cylindrical Mode Filtering for Far-field Antenna Measurements", Antenna Measurement Techniques Association, Cincinnati, USA, October 2025.

[2] S.F. Gregson, R.F. Dubrovka, C.G. Parini, "Compressed Sensing Based Spherical Mode Filtering Reflection Suppression for Far-Field Testing in Complex Electromagnetic Environments", European Conference on Antennas and Propagation, Stockholm, Sweden, April 2025.

[3] S. F. Gregson, J. Dupuy, C. G. Parini, A. C. Newell and G. E. Hindman, "Application of Mathematical Absorber Reflection Suppression to Far-field Antenna Measurements," *2011 Loughborough Antennas & Propagation Conference*, Loughborough, UK, 2011.

[4] Z. Chen, Y. Wang, "Generalized Cylindrical Mode Filtered Site VSWR for Above 18 GHz EMC Site Evaluation Using Compressed Sensing," EMC Europe 2023, Krakow.

[5] S.F. Gregson, C.G. Parini, A.C. Newell, "A General and Effective Mode Filtering Method for the Suppression of Clutter in Far-Field Antenna Measurements," AMTA Symposium, Williamsburg, VA, 2018.

[6] Z. Tian, S.F. Gregson, "Examination of the Effectiveness of Mode Orthogonalisation and Filtering for Scattering Suppression in Antenna Measurements Through Computational Electromagnetic Simulation," 13th European Conference on Antennas and Propagation (EuCAP 2019).

[7] Z. Chen, S. Gregson, Y. Wang, "Novel Application of Compressed Sensing in Cylindrical Mode Filtering for Far-Field Antenna Measurements," AMTA Symposium, Seattle, WA, 2023.

[8] G.J. Burke, A.J. Pogio, "User's Guide to the Numerical Electromagnetic Code (NEC) – Method of Moments," Naval Ocean System Center Technical Document 116, 3 vols., January 1981.

[9] J. E. Hansen (editor), "Spherical Near-Field Antenna Measurements", IET Press, London, UK 1988.